



Crystal structure of Kuzel's salt $3\text{CaO}\cdot\text{Al}_2\text{O}_3\cdot\frac{1}{2}\text{CaSO}_4\cdot\frac{1}{2}\text{CaCl}_2\cdot 11\text{H}_2\text{O}$ determined by synchrotron powder diffraction

Adel Mesbah^{a,f}, Michel François^b, Céline Cau-dit-Coumes^a, Fabien Frizon^a, Yaroslav Filinchuk^{c,1}, Fabrice Leroux^{d,g}, Johann Ravaux^e, Guillaume Renaudin^{f,g,*}

^a Commissariat à l'Energie Atomique et aux Energies Alternatives, CEA DEN/DTCD/SPDE, F-30207 Bagnols sur Cèze, France

^b Institut Jean Lamour, UMR 7198, Université Henri Poincaré, Nancy Université, F-54506 Vandoeuvre les Nancy, France

^c Swiss–Norwegian Beam Lines at ESRF, 6 rue Jules Horowitz, BP 220, F-38043 Grenoble, France

^d Clermont Université, Université Blaise Pascal, Laboratoire des Matériaux Inorganiques, BP 10448, F-63000 Clermont-Ferrand, France

^e Institut de Chimie Séparative de Marcoule, UMR 5257 CEA/CNRS/UM2/ENSCM, BP 17171, CEA Marcoule, F-30207 Bagnols-sur-Cèze, France

^f Clermont Université, ENSCCF, Laboratoire des Matériaux Inorganiques, BP 10448, F-63000 Clermont-Ferrand, France

^g CNRS, UMR 6002, LMI, F-63177 Aubière, France

ARTICLE INFO

Article history:

Received 9 November 2010

Accepted 19 January 2011

Keywords:

Kuzel's salt

X-ray diffraction (B)

Crystal structure (B)

ABSTRACT

The crystal structure of Kuzel's salt has been successfully determined by synchrotron powder diffraction. It crystallizes in the rhombohedral $R\bar{3}$ symmetry with $a = 5.7508$ (2) Å, $c = 50.418$ (3) Å, $V = 1444.04$ (11) Å³. Joint Rietveld refinement was realized using three X-ray powder patterns recorded with a unique wavelength and three different sample-to-detector distances. Kuzel's salt is the chloro-sulfoaluminate AFm phase and belongs to the layered double hydroxide (LDH) large family. Its structure is composed of positively charged main layer $[\text{Ca}_2\text{Al}(\text{OH})_6]^+$ and negatively charged interlayer $[\text{Cl}_{0.50}\cdot(\text{SO}_4)_{0.25}\cdot 2.5\text{H}_2\text{O}]^-$. Chloride and sulfate anions are ordered into two independent crystallographic sites and fill successive interlayer leading to the formation of a second-stage compound. The two kinds of interlayer have the compositions $[\text{Cl}\cdot 2\text{H}_2\text{O}]^-$ and $[(\text{SO}_4)_{0.5}\cdot 3\text{H}_2\text{O}]^-$. The crystal structure explains why chloride and sulfate anions are not substituted and why the formation of extended solid solution in the chloro-sulfate AFm system does not occur.

© 2011 Elsevier Ltd. All rights reserved.

1. Introduction

Calcium sulfoaluminate (CSA) cements may have a good potential to stabilize hazardous wastes such as heavy metals [1–8], ion exchange resins [9], aluminum-containing wastes [10] or radioactive streams containing high amounts of borate and sulfate ions [11]. Their outstanding confining properties are attributed to the structural flexibility of the two main hydrates formed, namely calcium monosulfoaluminate hydrate (an AFm phase [12]) and ettringite (an AFt phase [13]), which can accommodate many substitutions, both by cations and anions [14–18]. In this article, the focus is placed on chloride ions, which can be present as ³⁶Cl in many nuclear waste streams. AFm phases exhibit good capacities to bind chloride anions contrarily to AFt phases [15,19,20]. AFm phases belong to the lamellar double hydroxide (LDH) large family. The

crystal structure of AFm phases is composed of positively charged main layers $[\text{Ca}_2\text{Al}(\text{OH})_6]^+$ and negatively charged interlayers $[\text{X}\cdot n\text{H}_2\text{O}]^-$ where X is one monovalent anion or half a divalent anion. The following general formulae $3\text{CaO}\cdot\text{Al}_2\text{O}_3\cdot\text{CaX}_2\cdot n\text{H}_2\text{O}$ for a monovalent anion, or $3\text{CaO}\cdot\text{Al}_2\text{O}_3\cdot\text{CaX}\cdot n\text{H}_2\text{O}$ for a divalent anion, are generally used in cement chemistry. Several crystallographic studies have been performed on AFm compounds incorporating one type of anion only in the interlayer: SO_4^{2-} [12], Cl^- [21–23], CO_3^{2-} [24,25], NO_3^- [26,27], I^- [28,29] and Br^- [28,29]. Few crystallographic studies were devoted to bi anionic-AFm compounds formed by Cl^- – Br^- [29], CO_3^{2-} – OH^- [30] or CO_3^{2-} – Cl^- permutation [31–33].

The present study first aimed at providing a complete crystallographic description of the SO_4^{2-} – Cl^- bi anionic-AFm compounds – Kuzel's salt of composition $3\text{CaO}\cdot\text{Al}_2\text{O}_3\cdot\frac{1}{2}\text{CaCl}_2\cdot\frac{1}{2}\text{CaSO}_4\cdot 11\text{H}_2\text{O}$ (which differs from Kuzelite, the mineral name of monosulfoaluminate of composition $3\text{CaO}\cdot\text{Al}_2\text{O}_3\cdot\text{CaSO}_4\cdot 12\text{H}_2\text{O}$ [12]) – by powder X-ray diffraction data. H. J. Kuzel proposed a description of Kuzel's salt in 1966 [34,35], involving ordering of chloride and sulfate anions which fill alternatively successive interlayer regions. However, accurate crystallographic data are still missing. The second objective was to investigate the chloride to sulfate permutation in the chloro-sulfate AFm system in order to explain the absence of any extended solid solution, as previously noticed by several authors [20].

* Corresponding author at: Clermont Université, ENSCCF, Laboratoire des Matériaux Inorganiques, BP 10448, F-63000 Clermont-Ferrand, France. Tel.: +33 4 73 40 73 36; fax: +33 4 73 40 71 08.

E-mail address: guillaume.renaudin@ensccf.fr (G. Renaudin).

¹ Present address: Institute of Condensed Matter and Nanosciences, Université Catholique de Louvain, Place L. Pasteur 1, B-1348, Louvain-la-Neuve, Belgium.

2. Experimental section

2.1. Synthesis

Powder samples with nominal compositions $[\text{Ca}_2\text{Al}(\text{OH})_6] \cdot [\text{Cl}_{1-x}(\text{SO}_4)_{x/2} \cdot (2+x/2)\text{H}_2\text{O}]$ were synthesized in aqueous solution. The starting powders $\text{Ca}_3\text{Al}_2\text{O}_6$, $\text{CaCl}_2 \cdot 2\text{H}_2\text{O}$ (Aldrich, $\geq 99\%$) and $\text{CaSO}_4 \cdot 2\text{H}_2\text{O}$ (Aldrich, $\geq 99\%$) were mixed in pure boiled water (decarbonated) to reach a water/solid mass ratio of 50.

Two series of syntheses were prepared, each of them with $x = 0.25, 0.50$ and 0.75 . The first one was performed at room temperature for one month in closed polypropylene bottles, and the second one at 85°C for three weeks in closed Teflon reactors. The six suspensions were stored under nitrogen and continuous stirring. At the end of the experiments, the products were centrifuged twice in demineralised and decarbonated water before performing a third centrifugation with isopropanol. The obtained precipitates were subsequently dried in a desiccator, under slight vacuum, over potassium acetate ($\approx 20\%$ r.h.) at room temperature.

The three samples from the series synthesized at room temperature were named AFm- $[\text{Cl}_{3/4}(\text{SO}_4^{2-})_{1/8}]$ - 25°C , AFm- $[\text{Cl}_{1/2}(\text{SO}_4^{2-})_{1/4}]$ - 25°C , AFm- $[\text{Cl}_{1/4}(\text{SO}_4^{2-})_{3/8}]$ - 25°C for $x = 0.25, 0.50, 0.75$ respectively. The three samples from the series synthesized at 85°C were named AFm- $[\text{Cl}_{3/4}(\text{SO}_4^{2-})_{1/8}]$ - 85°C , AFm- $[\text{Cl}_{1/2}(\text{SO}_4^{2-})_{1/4}]$ - 85°C , AFm- $[\text{Cl}_{1/4}(\text{SO}_4^{2-})_{3/8}]$ - 85°C .

2.2. SEM analysis (EDS)

Scanning electron microscopy (SEM) analyses were performed with a field emission gun electron microscope (FEI QUANTA 200 ESEM FEG model) coupled with a Bruker SDD 5010 energy dispersive spectrometer (EDS). As the compounds to be analyzed may be damaged under the electron beam, the beam current was lowered by using a $30\ \mu\text{m}$ aperture, whereas the acceleration voltage was maintained at $15\ \text{kV}$ and the acquisition time limited to $30\ \text{s}$.

Kuzel's salt sample synthesized at room temperature was analyzed to check its chemical composition. It was prepared by dispersion in ethanol, deposited on a carbon holder, and fully coated with carbon. The particle sizes ranged between 0.5 and $20\ \mu\text{m}$. Fifty measurements were performed on one sample, and each analysis was recorded on different crystals. A statistical treatment of the chemical analyses allowed rejecting outliers.

2.3. Thermogravimetry analyses (TGA)

Thermogravimetric analyses (TGA) were performed with a Netzsch STA 409 PC instrument between 20°C and 1200°C under nitrogen atmosphere using a heating rate of $2^\circ\text{C}/\text{min}$. TGA were used to determine the amount of water contained in the interlayer region and to check the anionic stoichiometry.

2.4. Raman spectroscopy

Micro-Raman spectra were recorded at room temperature in the back scattering geometry using a Jobin-Yvon T64000 device. The spectral resolution, about $1\ \text{cm}^{-1}$, was obtained with an excitation source at $514.5\ \text{nm}$ (argon ion laser line, Spectra Physics 2017). The Raman detector was a charge coupled device (CCD) multichannel detector cooled down at $140\ \text{K}$ by liquid nitrogen. The laser beam was focussed onto the sample through an Olympus confocal microscope with $\times 100$ magnification. The laser spot was about $1\ \mu\text{m}^2$. The measured power at the sample level was kept low ($< 15\ \text{mW}$) in order to avoid any damage of the material. The Raman scattered light was collected with a microscope objective at 360° from the excitation and filtered with a holographic Notch filter before being dispersed by a single grating (1800 grooves per mm).

2.5. X-ray diffraction

2.5.1. Laboratory powder diffraction

Powder X-ray diffraction (PXRD) patterns were recorded using Cu $K\alpha$ radiation ($\lambda = 1.54184\ \text{\AA}$) on an X'Pert Pro PANalytical diffractometer, with θ - θ geometry, equipped with a X'Celerator solid detector and a Ni filter. PXRD patterns were recorded at room temperature in the interval $3^\circ < 2\theta < 120^\circ$, with a step size $\Delta 2\theta = 0.0167^\circ$ and a total counting time of about $3\ \text{h}$.

2.5.2. Synchrotron powder diffraction

Synchrotron powder diffraction data were recorded at the Swiss-Norwegian Beam Lines at ESRF (Grenoble, France) for the Kuzel's salt sample synthesized at 25°C ; i.e. AFm- $[\text{Cl}_{1/2}(\text{SO}_4^{2-})_{1/4}]$ - 25°C sample. White powder was introduced into a Lindeman capillary ($0.5\ \text{mm}$ by diameter). Data collection was performed at $295\ \text{K}$ with a MAR345 Image Plate detector by using a monochromatic wavelength ($\lambda = 0.70093\ \text{\AA}$). The calculated absorption coefficient $\mu \cdot R$ (μ = linear absorption coefficient, R = radius of the capillary) was estimated at 0.338 . Repetitive measurements showed the non-destructive nature of the X-ray dose. Three sample-to-detector distances were used ($150, 250$ and $400\ \text{mm}$) in order to combine the advantages of high structural and angular resolutions. The detector parameters and the wavelength were calibrated with NIST LaB₆ (660b). An instrumental resolution function was determined from the LaB₆ data for each sample-to-detector distance.

2.5.3. Indexation and Le-Bail procedure

Indexing was made for the pattern recorded with a sample-to-detector distance of $400\ \text{mm}$ (high angular resolution). Standard peak search method was used to locate the diffraction peak maxima with the Reflex program from Material Studio system software (Accelrys). The X-Cell indexing program allowing space group determination was used [36] and solution was found in rhombohedral $R\bar{3}$ space group. Proposed lattice parameters were $a = 5.758\ \text{\AA}$, and $c = 50.4313\ \text{\AA}$ (figure of merit FOM = $1/700$ for the 18 first reflections). A Le-Bail fitting was made using Fullprof [37]. The peak shape was described with the Thomson-Cox-Hastings function [38]. The profile matching refinement using the first pattern recorded with a sample-to-detector distance of $150\ \text{mm}$ (large angular range) led to the following good agreement factors: $R_p = 1.27\%$ and $R_{wp} = 1.53\%$ with $a = 5.7508(1)\ \text{\AA}$, $c = 50.4184(7)\ \text{\AA}$ and $V = 1444.02(2)\ \text{\AA}^3$. No superstructure peaks were observed, and the previously proposed hexagonal axis $c = 100.6\ \text{\AA}$ by H. J. Kuzel [34,35] was not considered at this stage of the study.

2.5.4. Structure solution and refinement strategy

The structure was solved by using the direct methods from the EXPO 2004 program [39] working on the extracted intensities from Le-Bail procedure. The centrosymmetric $R\bar{3}$ space group symmetry was confirmed, and not $R\bar{3}c$. The absence of the c glide mirror could be explained by the ordering of the anions: chlorides, and sulfur atoms from sulfate groups were located on the $3a$ and $3b$ Wyckoff sites respectively. The structure was refined with Fullprof program [37] using joint refinement from the three patterns. The model contained 11 atomic sites. Ow were water molecules (Ow1, Ow2: linked molecules, Ow3: weakly bonded molecules), O1 and O2 were the apical and basal oxygen atoms of the sulfate groups respectively. The refinement of 61 parameters (36 intensity dependent parameters, 25 profile parameters) including: 1 zero shift, 1 scale factor, 2 lattice parameters, 13 atomic coordinates, 9 temperature factors, led to the final agreement factors $R_{\text{Bragg}1,2,3}(\%) = 7.01, 6.78, 6.47$, and $R_{\text{F}1,2,3}(\%) = 7.87, 6.98, 5.69$ for the sample-to-detector distances of $150, 250$ and $400\ \text{mm}$ respectively. Refinement parameters are collected in Table 1.

The four following constraints on occupancy factors were used: $\text{occ}(\text{S}) = 0.5$, $\text{occ}(\text{O1}) = \text{occ}(\text{O2}) = 0.25$, $\text{occ}(\text{Ow3}) = 0.1667$. It

allowed fixing the composition to $3\text{CaO}\cdot\text{Al}_2\text{O}_3\cdot 1/2\text{CaSO}_4\cdot 1/2\text{CaCl}_2\cdot 11\text{H}_2\text{O}$, in agreement with TGA and EDS results.

The four following soft restraints on interatomic distances were also applied: $d_{\text{S-O}1} = d_{\text{S-O}2} = 1.45(5) \text{ \AA}$, $d_{\text{Ca}1\text{-Ow}1} = d_{\text{Ca}2\text{-Ow}2} = 2.50(5) \text{ \AA}$.

Constraints and restraints were used to take into account the complex nature of the two kinds of interlayer regions, as well as the presence of disorder in the interlayer due to statistical distribution between one sulfate group and two water molecules on the Ow3 site, and to the orientational disorder of the sulfate tetrahedra.

3. Results and discussion

3.1. Kuzel's salt characterization

The Kuzel's salt sample synthesized at room temperature, AFm- $[\text{Cl}_{1/2}(\text{SO}_4^{2-})_{1/4}]$ -25 °C ($x = 0.5$), was the only single phase material (Fig. 1, top). This powder was used for the X-ray synchrotron powder diffraction measurement. The AFm- $[\text{Cl}_{1/2}(\text{SO}_4^{2-})_{1/4}]$ -85 °C sample contained small amount of calcium monosulfoaluminate hydrate (Fig. 1, bottom). The $x = 0.25$ samples (AFm- $[\text{Cl}_{3/4}(\text{SO}_4^{2-})_{1/8}]$ -25 °C and AFm- $[\text{Cl}_{3/4}(\text{SO}_4^{2-})_{1/8}]$ -85 °C) mainly contained Kuzel's salt and Friedel's salt. Finally, the $x = 0.75$ samples (AFm- $[\text{Cl}_{1/4}(\text{SO}_4^{2-})_{3/8}]$ -25 °C and AFm- $[\text{Cl}_{1/4}(\text{SO}_4^{2-})_{3/8}]$ -85 °C) comprised a mixture of Kuzel's salt and a sulfate-rich phase (mainly ettringite for the synthesis at room temperature, and monosulfoaluminate for the synthesis at 85 °C; see Fig. 1).

3.1.1. Kuzel's salt chemical composition

The chemical composition of Kuzel's salt was determined by combining SEM-EDS analyses and TGA. The simultaneous presence of the two anions was clearly evidenced, with a calculated anionic $\text{Cl}^-/\text{SO}_4^{2-}$ molar ratio of 1.8 for the Kuzel's salt synthesized at room temperature. The Ca/Al/Cl/S atomic ratios were measured as 2.00/1.00/0.46/0.26; which agreed fairly well with the electroneutrality of the compound.

The first weight loss recorded by TGA (see Fig. 2) between 25 and 300 °C corresponded to the departure of the eleven water molecules per formula unit $3\text{CaO}\cdot\text{Al}_2\text{O}_3\cdot 1/2\text{CaSO}_4\cdot 1/2\text{CaCl}_2\cdot 11\text{H}_2\text{O}$ (calc = 33.90%, exp = 34.08%). Dehydration and dehydroxylation were mostly completed at 300 °C. The second weight loss between 450 °C and 900 °C corresponded to the departure of chloride (calc = 6.07%, exp = 7.53%), and the last weight loss between 1000 °C and 1200 °C was attributed to the decomposition of sulfate (calc = 6.36% for departure of SO_3 ,

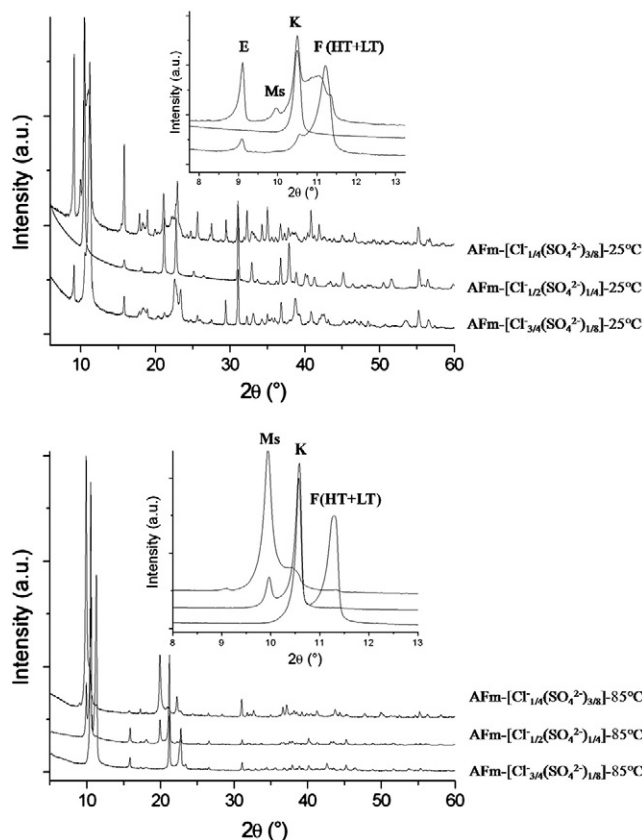


Fig. 1. Laboratory PXRD patterns of the six powdered AFm- $[\text{Cl}_{3/4}(\text{SO}_4^{2-})_{1/8}]$, AFm- $[\text{Cl}_{1/2}(\text{SO}_4^{2-})_{1/4}]$ and AFm- $[\text{Cl}_{1/4}(\text{SO}_4^{2-})_{3/8}]$ samples; bottom (the 85 °C series) and top (the 25 °C series). E, Ms, K and F, respectively refer to ettringite, monosulfoaluminate, Kuzel's salt and Friedel's salt.

exp = 6.94%) by referring to the temperature of decomposition of anhydrite CaSO_4 . The residual powder, obtained after calcinations at 1200 °C, was analyzed by PXRD. It was composed of a mixture of lime (CaO) and mayenite ($\text{Ca}_{12}\text{Al}_{14}\text{O}_{33}$) – PDF files 43–1001 and 48–1882 respectively – in agreement with SEM results and TGA interpretations.

The apparent minor underestimation of the chloride content could be explained by the carbonate contamination of our powders. This observation was confirmed by Raman spectroscopy with vibration at 1086 cm^{-1} (Fig. 3) which is characteristic of weakly bonded carbonate anion in the center of the interlayer region [31,32]. The carbonate contamination explained also the simultaneous presence of the low temperature (LT–) and the high temperature (HT–) polymorphs of Friedel's salt in both AFm- $[\text{Cl}_{3/4}(\text{SO}_4^{2-})_{1/8}]$ samples, as indicated by the LT + HT notations in Fig. 1. It has been shown that

Table 1

Crystal and structure refinement data of Kuzel's salt. Standard deviations are indicated in bracket.

Compound	Kuzel's salt
Formula	$3\text{CaO}\cdot\text{Al}_2\text{O}_3\cdot 0.5\text{CaSO}_4\cdot 0.5\text{CaCl}_2\cdot 11\text{H}_2\text{O}$
Structural formula	$[\text{Ca}_2\text{Al}(\text{OH})_6]^+[\text{O}25\text{SO}_4\cdot 0.5\text{Cl}\cdot 2.5\text{H}_2\text{O}]^-$
Calculated formula weight ($\text{g}\cdot\text{mol}^{-1}$)	583.919
T(K)	293 K
System	Rhombohedral
Space group	$R\bar{3}$
a (Å)	5.7508(2)
c (Å)	50.4185(29)
V (Å ³)	1444.04(11)
Z/Dx ($\text{g}\cdot\text{cm}^{-3}$)	3/2.014
Wavelength (Å)	0.70093
Angular range 2θ (°) 1, 2, 3	3.75–48.91, 3.66–34.64, 3.66–23.37
Nobs 1, 2, 3	1473, 1443, 1338
Nref 1, 2, 3	652, 215, 77
R_p 1, 2, 3 (%)	2.01, 2.58, 2.41
R_{wp} 1, 2, 3 (%)	2.62, 3.52, 3.93
R_{Bragg} 1, 2, 3 (%)	7.01, 6.78, 6.47
R_f 1, 2, 3 (%)	7.87, 6.98, 5.69
N of profile parameters	25
N intensity dependent parameters	36

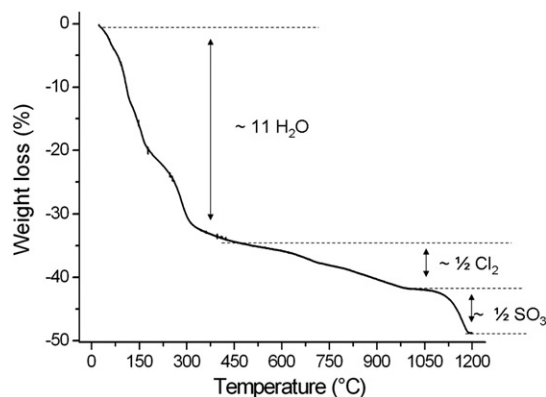


Fig. 2. TGA curve of Kuzel's salt from AFm- $[\text{Cl}_{1/2}(\text{SO}_4^{2-})_{1/4}]$ -25 °C sample.

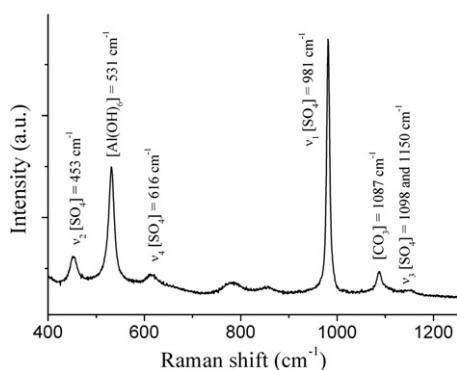


Fig. 3. Raman spectra of the Kuzel's salt in the range 400–1250 cm^{-1} showing the modes of vibration of sulfate, carbonate and $[\text{Al}(\text{OH})_6]$ groups.

carbonate to chloride substitution is easily realized in Friedel's salt and lead to a decrease of the temperature of transition [31,32]; this weak carbonate contamination explains the simultaneous presence of both polymorphs.

3.1.2. Crystal structure description of Kuzel's salt

Joint Rietveld refinement (Fig. 4 shows the Rietveld plot obtained for one pattern) led to complete description of the Kuzel's salt structure. Refined atomic parameters are given in Table 2. A general representation of the Kuzel's salt structure is presented in Fig. 5 along the [100] direction. The layered feature of this bi-anionic AFm compound was clearly maintained, likewise the previously described chloro-carboaluminate AFm compound [32]. Main layer in Kuzel's salt structure was typical of the AFm family: the oxygen coordination numbers of Al, respectively Ca, cation were six ($6 \times 1.92 \text{ \AA}$), respectively seven ($3 \times 2.37 \text{ \AA}$, $3 \times 2.46 \text{ \AA}$ and $1 \times 2.50 \text{ \AA}$ for Ca1, and $3 \times 2.39 \text{ \AA}$, $3 \times 2.51 \text{ \AA}$ and $1 \times 2.50 \text{ \AA}$ for Ca2). The seventh neighbors of the Ca atoms (Ca1 and Ca2 sites) were bonded water molecules located in the Ow1 and Ow2 sites. Selected interatomic distances are listed in Table 3. Nevertheless, a major structural feature appeared for the first time in the Kuzel's salt structure: anionic ordering led to the formation of two kinds of interlayer regions. We observed the succession of interlayer filled by chloride anions only with composition $[\text{Cl} \cdot 2\text{H}_2\text{O}]^-$ (bottom interlayer in Fig. 5), and interlayer filled by sulfate anions and weakly bonded water molecules with composition $[(\text{SO}_4)_{0.5} \cdot 3\text{H}_2\text{O}]^-$ (top interlayer in Fig. 5). Such an alternate in the interlayer filling led to a second-stage layered compound, unlike the chloro-carboaluminate AFm compound [32] which presents a single type of interlayer region simultaneously containing the two Cl^- and CO_3^{2-} anions (as usually observed in AFm phases). The staging feature of Kuzel's salt was due to the ordering of the two anions into specific and successive interlayers. Such an ordering

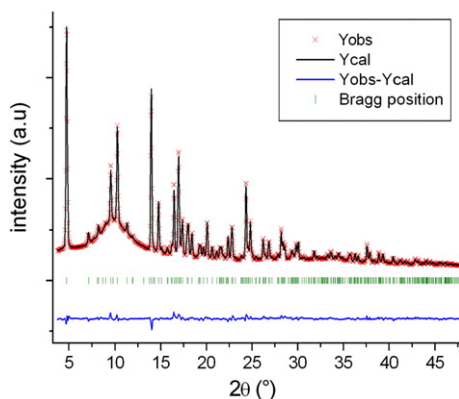


Fig. 4. Rietveld plot for the synchrotron powder pattern recorded on AFm- $[\text{Cl}_{1/2}(\text{SO}_4^{2-})_{1/4}]$ -25 °C sample with a sample-to-detector distance of 150 mm ($\lambda = 0.70093 \text{ \AA}$).

Table 2

Atomic coordinates and equivalent isotropic displacement parameters ($\text{\AA}^2 \times 10^{-3}$) for Kuzel's salt. Standard deviations are indicated in bracket.

Atom	Wyckoff site	x	y	z	U_{eq}	Occupancy
Al	6c	2/3	1/3	0.0784(1)	7.8(14)	1.0
Ca1	6c	0.0	0.0	0.0901(1)	15.0(13)	1.0
Ca2	6c	0.0	0.0	0.4000(1)	26.0(17)	1.0
Oh1	18f	0.4180(10)	0.3868(15)	0.0993(1)	6(3)	1.0
Oh2	18f	0.9126(10)	0.2708(13)	0.0581(1)	5(2)	1.0
Ow1	6c	0.0	0.0	0.1397(1)	50(5)	1.0
Ow2	6c	0.0	0.0	0.3504(1)	49(5)	1.0
Cl	3a	0.0	0.0	0.0	112(4)	1.0
S	3b	0.0	0.0	0.5	48(5)	0.5 (–)
O1	6c	0.0	0.0	0.4712 (1)	$=U_{\text{eq}}(\text{S})$	$=U_{\text{eq}}(\text{S})$
O2	18f	0.2689(13)	0.185(3)	0.5094(3)	$=U_{\text{eq}}(\text{S})$	0.25 (–)
Ow3	18f	$=x(\text{O2})$	$y(\text{O2})$	$=z(\text{O2})$	$=U_{\text{eq}}(\text{S})$	0.166 (–)

into successive interlayer regions has already been observed in layered double hydroxide (LDH) compounds, but in the presence of mixed organic–inorganic anions [40]. According to the authors' knowledge, Kuzel's salt is the first described staging AFm structure, although it was already postulated by Kuzel in 1966 [34]. Kuzel's salt and monosulfoaluminate (i.e. Kuzelite) [12] structures are both described in the rhombohedral $R\bar{3}$ symmetry. However, due to staging, the c hexagonal axis for Kuzel's salt (50.418 (3) \AA) is about twice that of monosulfoaluminate ($c = 26.745 \text{ \AA}$ [12]). The two-stage feature of Kuzel's salt $[\text{Ca}_2\text{Al}(\text{OH})_6] \cdot [\text{Cl}_{0.50} \cdot (\text{SO}_4)_{0.25} \cdot 2.5\text{H}_2\text{O}]$ structure results from the perfect intercalation of the structures of the two end-members: monosulfoaluminate with composition $[\text{Ca}_2\text{Al}(\text{OH})_6] \cdot [(\text{SO}_4)_{0.5} \cdot 3\text{H}_2\text{O}]$ and Friedel's salt with composition $[\text{Ca}_2\text{Al}(\text{OH})_6] \cdot [\text{Cl} \cdot 2\text{H}_2\text{O}]$.

The sulfate-containing interlayer in Kuzel's salt, as well as in monosulfoaluminate structure, presents similar types of disorders: 1/ a statistical disorder between one sulfate anion and two water molecules (O2 and Ow3 positions located on the same general position), and 2/ an orientational disorder of tetrahedral sulfate anions (up and down). Raman spectrum from Kuzel's salt (Fig. 3) presents the sulfate modes of vibration in perfect accordance with band positions previously observed for monosulfoaluminate [41]: ν_1 mode at 981 cm^{-1} (compared to 982 cm^{-1} for monosulfoaluminate), ν_2 mode at 453 cm^{-1} (compared to 453 cm^{-1}), ν_3 modes at 1098 and 1150 cm^{-1} (compared to 1095 and 1154 cm^{-1}) and ν_4 mode at 616 cm^{-1} (compared to 615 cm^{-1}). This correlation evidences the equivalent sulfate-containing interlayer in both Kuzel's salt and monosulfoaluminate structures.

Low temperatures PXRD measurements have been performed down to 100 K (not shown here) to check the presence of an eventual structure transition. Unlike observed in Friedel's salt, the chloride-

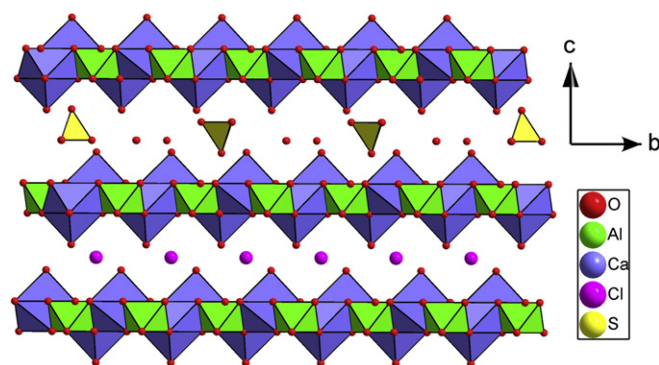


Fig. 5. General representation of the Kuzel's salt structure along [100]. For clarity reasons, distribution between one sulfate group and two water molecules, and orientation disorder of sulfate groups (up and down) were ordered.

Table 3

Selected interatomic distances in Kuzel's salt structure. Standard deviations are indicated in bracket.

Kuzel's salt		
Al	3×Oh1	1.921(1)
	3×Oh2	1.921(1)
Ca1	3×Oh1	2.366(1)
	3×Oh2	2.464(1)
Ca2	Ow1	2.502(1)
	3×Oh2	2.392(5)
	3×Oh1	2.513(5)
	Ow2	2.502(8)
S	O1	1.451(9)
	3×O2	1.452(7)
O1	3×Oh1	2.721(1)
	3×Ow1	3.323(4)
O2 (Ow3)	Ow1	2.716(2)
	Ow1	2.749(2)
	Ow1	3.306(1)
Cl	Oh1	3.082(1)
	6×Ow2	3.432(1)
	6×Oh2	3.472(1)

containing interlayer did not induce a transition from rhombohedral to monoclinic symmetry when cooling (at least down to 100 K).

3.2. The $\text{Ca}_3\text{Al}_2\text{O}_3\text{--CaCl}_2\text{--CaSO}_4\text{--H}_2\text{O}$ system

The possibilities to exchange chloride by sulfate in one kind of interlayer or to exchange sulfate by chloride in the other kind of interlayer were investigated by the syntheses with $x=0.25$ and $x=0.75$ (on both side of the Kuzel's salt stoichiometry) at room temperature and 85 °C. Laboratory X-ray powder patterns corresponding to the six samples AFm- $[\text{Cl}_{3/4}(\text{SO}_4^{2-})_{1/8}]$ -25 °C, AFm- $[\text{Cl}_{1/2}(\text{SO}_4^{2-})_{1/4}]$ -25 °C, AFm- $[\text{Cl}_{1/4}(\text{SO}_4^{2-})_{3/8}]$ -25 °C, AFm- $[\text{Cl}_{3/4}(\text{SO}_4^{2-})_{1/8}]$ -85 °C, AFm- $[\text{Cl}_{1/2}(\text{SO}_4^{2-})_{1/4}]$ -85 °C and AFm- $[\text{Cl}_{1/4}(\text{SO}_4^{2-})_{3/8}]$ -85 °C are presented in Fig. 1.

3.2.1. Mineralogical composition of the 25 °C series

Qualitative analyses of the X-ray powder patterns showed multiphased powders. Four different hydrates were identified: monosulfoaluminate, Kuzel's salt, Friedel's salt (the two LT- and HT-polymorphs were present simultaneously), and ettringite (the only AFt phase). The stabilization of the two polymorphs of Friedel's salt was probably due to a weak carbonate contamination [31,32]. The major phase in the AFm- $[\text{Cl}_{3/4}(\text{SO}_4^{2-})_{1/8}]$ -25 °C sample was Friedel's salt. Kuzel's salt and ettringite were present as minor phases, whereas monosulfoaluminate was not observed. The AFm- $[\text{Cl}_{1/4}(\text{SO}_4^{2-})_{3/8}]$ -25 °C sample contained the four hydrates. Ettringite and Kuzel's salt predominated over monosulfoaluminate.

3.2.2. Mineralogical composition of the 85 °C series

When synthesis was performed at 85 °C, the sulfate-rich AFm- $[\text{Cl}_{1/4}(\text{SO}_4^{2-})_{3/8}]$ -85 °C sample was mostly composed of monosulfoaluminate, with smaller amount of Kuzel's salt. Ettringite was no longer observed because of the decrease of its stability domain at 85 °C [42]. The AFm- $[\text{Cl}_{3/4}(\text{SO}_4^{2-})_{1/8}]$ -85 °C sample contained the two chloride-containing AFm phases: Kuzel's salt and Friedel's salt (mixture of the two LT- and HT-polymorphs). The AFm- $[\text{Cl}_{1/2}(\text{SO}_4^{2-})_{1/4}]$ -85 °C sample was mostly composed of the Kuzel's salt, with small amount of monosulfoaluminate.

These results, in agreement with those of Balonis et al. [20], clearly show that extended anionic permutation into the two kinds of interlayer regions is not allowed in the Kuzel's salt structure. The staging feature of Kuzel's salt certainly explains the difficulties to substitute chloride and sulfate: the modification in one kind of interlayer involves a modification in the other kind of interlayer in order to preserve the electroneutrality of the compound. The second-

stage feature of Kuzel's salt implies that each interlayer should be mono-anionic.

4. Conclusion

The crystal structure of the Kuzel's salt with general formula $3\text{CaO}\cdot\text{Al}_2\text{O}_3\cdot 1/2\text{CaSO}_4\cdot 1/2\text{CaCl}_2\cdot 11\text{H}_2\text{O}$ was solved and refined by synchrotron powder diffraction method. This was the first AFm structure determined *ab initio* from X-ray powder diffraction data using direct method with a full crystal structure description reached by Rietveld refinement. Kuzel's salt is a two-stage layered compound with two distinct interlayers, which are alternatively filled by chloride anions only (for one kind of interlayer) and by sulfate anions and water molecules (for the other kind of interlayer). Kuzel's salt structure is composed of the perfect intercalation of the Friedel's salt structure and the monosulfoaluminate structure (the two end-members of the studied bi-anionic AFm compound). The structural properties of Kuzel's salt explain the absence of extended chloride to sulfate or sulfate to chloride substitution.

Acknowledgments

Laurent Petit, from Electricité de France, is deeply acknowledged for his support of the project. The authors also thank SNBL for the in-house beam time allocation.

References

- [1] V. Albino, R. Cioffi, M. Marroccoli, L. Santoro, Potential application of ettringite generating systems for hazardous waste stabilization, *Journal of Hazardous Materials* 51 (1–3) (1996) 241–252.
- [2] R. Berardi, R. Cioffi, L. Santoro, Chemical effects of heavy metals on the hydration of calcium sulfoaluminate $4\text{CaO}\cdot 3\text{Al}_2\text{O}_3\cdot \text{SO}_3$, *Journal of Thermal Analysis* 50 (3) (1997) 393–400.
- [3] S. Berger, C. Cau Dit Coumes, P. Le Bescop, D. Damidot, Hydration of calcium sulfoaluminate cement by a ZnCl_2 solution: investigation at early age, *Cement and Concrete Research* 39 (12) (2009) 1180–1187.
- [4] C.A. Luz, J. Pera, M. Cheriaf, J.C. Rocha, Behaviour of calcium sulfoaluminate cement in presence of high concentrations of chromium salts, *Cement and Concrete Research* 37 (4) (2007) 624–629.
- [5] C.A. Luz, J.C. Rocha, M. Cheriaf, J. Pera, Use of sulfoaluminate cement and bottom ash in the solidification/stabilization of galvanic sludge, *Journal of Hazardous Materials* 136 (3) (2006) 837–845.
- [6] C.A. Luz, J.C. Rocha, M. Cheriaf, J. Pera, Valorization of galvanic sludge in sulfoaluminate cement, *Construction and Building Materials* 23 (2) (2009) 595–601.
- [7] J. Péra, J. Ambroise, M. Chabannet, Valorization of automotive shredder residue in building materials, *Cement and Concrete Research* 34 (4) (2004) 557–562.
- [8] S. Peysson, J. Péra, M. Chabannet, Immobilization of heavy metals by calcium sulfoaluminate cement, *Cement and Concrete Research* 35 (12) (2005) 2261–2270.
- [9] J. Li, J. Wang, Advances in cement solidification technology for waste radioactive ion exchange resins: a review, *Journal of Hazardous Materials* 135 (1–3) (2006) 443–448.
- [10] Q. Zhou, N.B. Milestone, M. Hayes, An alternative to Portland Cement for waste encapsulation—the calcium sulfoaluminate cement system, *Journal of Hazardous Materials* 136 (1 SPEC. ISS.) (2006) 120–129.
- [11] C. Cau Dit Coumes, S. Courtois, S. Peysson, J. Ambroise, J. Pera, Calcium sulfoaluminate cement blended with OPC: a potential binder to encapsulate low-level radioactive slurries of complex chemistry, *Cement and Concrete Research* 39 (9) (2009) 740–747.
- [12] R. Allmann, Refinement of the hybrid layer structure hexahydroxoaluminocalcium hemisulfate trihydrate ($\text{Ca}_2\text{Al}(\text{OH})_6\cdot(1/2\text{SO}_4\cdot 3\text{H}_2\text{O})$), *Neues Jahrbuch für Mineralogie, Monatshefte* (1977).
- [13] A.E. Moore, H.F.W. Taylor, Crystal structure of ettringite, *Acta Crystallographica, Section B* 26 (4) (1970) 386–393.
- [14] M. Chrysochoou, D. Dermatas, Evaluation of ettringite and hydrocalumite formation for heavy metal immobilization: literature review and experimental study, *Journal of Hazardous Materials* 136 (1 SPEC. ISS.) (2006) 20–33.
- [15] F.P. Glasser, A. Kindness, S.A. Stronach, Stability and solubility relationships in AFm phases: Part I. Chloride, sulfate and hydroxide, *Cement and Concrete Research* 29 (6) (1999) 861–866.
- [16] M.L.D. Gougar, B.E. Scheetz, D.M. Roy, Ettringite and C–S–H portland cement phases for waste ion immobilization: a review, *Waste Management* 16 (4) (1996) 295–303.
- [17] P. Kumarathasan, G.J. McCarthy, D.J. Hassett, D. Pflughoeftasset, Oxyanion substituted ettringites: synthesis and characterization; and their potential role in immobilization of As, B, Cr, Se and V, *Materials Research Society Symposium Proceedings* (1990) 83–104.

- [18] G.J. McCarthy, D.J. Hassett, J.A. Bender, Synthesis, crystal chemistry and stability of ettringite, a material with potential applications in hazardous waste immobilization, *Materials Research Society Symposium Proceedings* (1992) 129–140.
- [19] H. Hirao, K. Yamada, H. Takahashi, H. Zibara, Chloride binding of cement estimated by binding isotherms of hydrates, *Journal of Advanced Concrete Technology* 3 (1) (2005) 77–84.
- [20] M. Balonis, B. Lothenbach, G. Le Saout, F.P. Glasser, Impact of chloride on the mineralogy of hydrated Portland cement systems, *Cement and Concrete Research* 40 (7) (2010) 1009–1022.
- [21] A. Terzis, S. Filippakis, K. H.J., H. Bruzlauff, The crystal structure of $\text{Ca}_2\text{Al}(\text{OH})_6\text{Cl}\cdot 2\text{H}_2\text{O}$, *Zeitschrift für Kristallographie* 181 (1–4) (1987) 29.
- [22] J.P. Rapin, G. Renaudin, E. Elkaim, M. François, Structural transition of Friedel's salt $3\text{CaO}\cdot\text{Al}_2\text{O}_3\cdot\text{CaCl}_2\cdot 10\text{H}_2\text{O}$ studied by synchrotron powder diffraction, *Cement and Concrete Research* 32 (4) (2002) 513–519.
- [23] G. Renaudin, F. Kubel, J.P. Rivera, M. François, Structural phase transition and high temperature phase structure of Friedel's salt, $3\text{CaO}\cdot\text{Al}_2\text{O}_3\cdot\text{CaCl}_2\cdot 10\text{H}_2\text{O}$, *Cement and Concrete Research* 29 (12) (1999) 1937–1942.
- [24] M. François, G. Renaudin, O. Evrard, A cementitious compound with composition $3\text{CaO}\cdot\text{Al}_2\text{O}_3\cdot\text{CaCO}_3\cdot 11\text{H}_2\text{O}$, *Acta Crystallographica. Section C: Crystal Structure Communications* 54 (9) (1998) 1214–1217.
- [25] G. Renaudin, M. François, O. Evrard, Order and disorder in the lamellar hydrated tetracalcium monocarboaluminate compound, *Cement and Concrete Research* 29 (1) (1999) 63–69.
- [26] G. Renaudin, M. François, The lamellar double-hydroxide (LDH) compound with composition $3\text{CaO}\cdot\text{Al}_2\text{O}_3\cdot\text{Ca}(\text{NO}_3)_2\cdot 10\text{H}_2\text{O}$, *Acta Crystallographica. Section C: Crystal Structure Communications* 55 (6) (1999) 835–838.
- [27] G. Renaudin, J.P. Rapin, B. Humbert, M. François, Thermal behaviour of the nitrated AFm phase $\text{Ca}_4\text{Al}_2(\text{OH})_{12}(\text{NO}_3)_2\cdot 4\text{H}_2\text{O}$ and structure determination of the intermediate hydrate $\text{Ca}_4\text{Al}_2(\text{OH})_{12}(\text{NO}_3)_2\cdot 2\text{H}_2\text{O}$, *Cement and Concrete Research* 30 (2) (2000) 307–314.
- [28] J.P. Rapin, A. Walcarius, G. Lefevre, M. François, A double-layered hydroxide, $3\text{CaO}\cdot\text{Al}_2\text{O}_3\cdot\text{CaI}_2\cdot 10\text{H}_2\text{O}$, *Acta Crystallographica. Section C: Crystal Structure Communications* 55 (12) (1999) 1957–1959.
- [29] G. Renaudin, J.P. Rapin, E. Elkaim, M. François, Polytypes and polymorphs in the related Friedel's salt $(\text{Ca}_2\text{Al}(\text{OH})_6)_x(\text{X}\cdot 2\text{H}_2\text{O})_y$ -halide series, *Cement and Concrete Research* 34 (10) (2004) 1845–1852.
- [30] R. Fischer, H.J. Kuzel, Reinvestigation of the system $\text{C}_4\text{A}\cdot n\text{H}_2\text{O}-\text{C}_4\text{A}\cdot\text{CO}_2\cdot n\text{H}_2\text{O}$, *Cement and Concrete Research* 12 (4) (1982) 517–526.
- [31] A. Mesbah, C. Cau Dit Coumes, F. Frizon, F. Leroux, J. Ravaux, G. Renaudin, A new investigation of the $\text{Cl}^- - \text{CO}_3^{2-}$ substitution in AFm phases, *Journal of the American Ceramic Society* (2010), doi:10.1111/j.1551-2916-2010-04305.x.
- [32] A. Mesbah, J.P. Rapin, M. François, C. Cau-dit-coumes, F. Frizon, F. Leroux, G. Renaudin, Crystal structures and phase transition of cementitious bianionic AFm- $(\text{Cl}^-, \text{CO}_3^{2-})$ compounds, *Journal of the American Ceramic Society* 94 (1) (2011) 262–269.
- [33] M. Sacerdoti, E. Passaglia, Hydrocalumite from Latium, Italy: its crystal structure and relationship with related synthetic phases, *Neues Jahrbuch für Mineralogie Monatshefte* 10 (1988) 462–475.
- [34] H.J. Kuzel, *N. Jb. Miner. Mh* (1966) 193–200.
- [35] H.J. Kuzel, *Zement Kalk Gips* 21 (1968) 463–469.
- [36] M.A. Neumann, X-Cell: a novel indexing algorithm for routine tasks and difficult cases, *Journal of Applied Crystallography* 36 (2) (2003) 356–365.
- [37] J. Rodriguez-Carvajal, Recent advances in magnetic structure determination by neutron powder diffraction, *Physica B: Condensed Matter* 192 (1–2) (1993) 55–69.
- [38] L.W. Finger, D.E. Cox, A.P. Jephcoat, Correction for powder diffraction peak asymmetry due to axial divergence, *Journal of Applied Crystallography* 27 (pt 6) (1994) 892–900.
- [39] A. Altomare, M. Camalli, C. Cuocci, I. Da Silva, C. Giacobozzo, A.G.G. Moliterni, R. Rizzi, Space group determination: improvements in EXPO2004, *Journal of Applied Crystallography* 38 (5) (2005) 760–767.
- [40] C. Taviot-Guého, F. Leroux, C. Payen, J.P. Besse, Cationic ordering and second-staging structures in copper-chromium and zinc-chromium layered double hydroxides, *Applied Clay Science* 28 (1–4 SPEC. ISS.) (2005) 111–120.
- [41] G. Renaudin, R. Segni, D. Mentel, J.-M. Nedelec, F. Leroux, C. Taviot-Gueho, A Raman study of the sulfated cement hydrates: ettringite and monosulfoaluminate, *Journal of Advanced Concrete Technology* 5 (3) (2007) 299–312.
- [42] D. Damidot, F.P. Glasser, Thermodynamic investigation of the $\text{CaO}^- - \text{Al}_2\text{O}_3^- - \text{CaSO}_4 - \text{H}_2\text{O}$ system at 50 °C and 85 °C, *Cement and Concrete Research* 22 (6) (1992) 1179–1191.